DYNAMIC LIFETIME IMAGING BASED ON PHOTOLUMINESCENCE MEASUREMENTS

Sandra Herlufsen[1], Klaus Ramspeck[1,3], David Hinken[1], Arne Schmidt[1], Jens Müller[1],
Karsten Bothe[1], Jan Schmidt[1], and Rolf Brendel[1,2]
[1]Institute for Solar Energy Research Hamelin (ISFH), Am Ohrberg 1, D-31860 Emmerthal, Germany
Tel: +49 5151 999 414; Fax: +49 5151 999 400; Email: herlufsen@isfh.de
[2]Institute for Solid-State Physics, Leibniz University Hannover, Appelstraße 2, D-30167 Hannover, Germany
[3]Now with SCHOTT Solar AG, Carl-Zeiss-Str. 4, D-63755 Alzenau, Germany

ABSTRACT: We report on calibration-free photoluminescence carrier lifetime imaging for the examination of crystalline silicon wafers. The photoluminescence measurements are performed using an indium gallium arsenide (InGaAs) camera. The carrier lifetime is determined from the time dependent luminescence emission for a modulated optical excitation. A ratio, including four photoluminescence images, acquired at different times during the modulated excitation, is calculated and found to depend only on the camera integration time and the effective carrier lifetime. Therefore, the carrier lifetime is unambiguously determined by this ratio without the knowledge of any additional wafer properties. The carrier lifetime is obtained locally by comparing the experimentally determined ratio with the simulated ratio for every image pixel. We demonstrate the applicability of the dynamic photoluminescence lifetime imaging technique to multicrystalline silicon wafers by comparison with microwave-detected photoconductance decay and quasi steady-state photoconductance decay measurements.
Keywords: Lifetime, Silicon, Photoluminescence, Imaging

1 INTRODUCTION

Testing the electronic properties of crystalline silicon (Si) is highly demanded for quality control in solar cell production. One of the key parameters for the investigation of silicon wafers is the carrier lifetime. Particularly in the case of multicrystalline silicon (mc-Si), spatially resolved information of the lifetime is of utmost importance, as this material typically has strongly inhomogeneous recombination properties. Thus, camera-based approaches are highly preferable.

Up to now, camera-based photoluminescence (PL) techniques for determining carrier lifetimes have exclusively been used under steady-state conditions [1-5]. For the conversion of the measured luminescence signal into the carrier lifetime, a reliable calibration procedure is required. One approach [3, 4] relates the luminescence emission to the excess carrier density determined from calibrated conductivity measurements carried out in the same setup. Unfortunately, this procedure relies on the precise knowledge of the dopant density of the sample, the wafer thickness and the validity of the underlying carrier mobility model. Alternatively, a calibration procedure based on calculations of the total number of emitted photons was recently suggested [5]. However, the optical properties of the sample have to be well-known to successfully apply this technique. Thus, a calibration-free approach enabling fast carrier lifetime imaging with a high spatial resolution would be of great advantage.

A calibration-free analysis can be realized by evaluating the time dependence of a physical quantity related to the excess carrier density. This quantity might be the conductivity [6], the reflected microwave power [7] or the luminescence emission under optical excitation. On the basis of measurements of the free carrier emission using an infrared camera, Ramspeck et al. [8] introduced the dynamic infrared lifetime mapping (dynamic ILM) technique. The aim of this work is to adapt this approach for dynamic camera-based photoluminescence (dynamic PL) measurements. The main advantages of PL measurements compared to ILM measurements are: (a) PL measurements are weakly influenced by measurement artefacts such as trapping [9, 10] or depletion region modulation [11], (b) they can be easily performed at room temperature.

2 THEORY

The dynamic PL lifetime technique is based on two elementary equations. The first expresses the relation between excess carrier density Δn and PL signal I_{PL}:

$$I_{PL} \propto \Delta n N_{dop} + \Delta n^2 \qquad (1)$$

with N_{dop} as the dopant density [12]. The second equation describes the time-dependence of the excess carrier density Δn in the wafer, based on the continuity equation:

$$d\Delta n(t) / dt = G - \Delta n(t) / \tau_{eff}, \qquad (2)$$

where G is the generation rate and τ_{eff} is the effective carrier lifetime. Equation (2) has to be solved for two cases: $\Delta n_{rise}(t)$, after a light source is switched on (constant $G > 0$) and $\Delta n_{fall}(t)$, after a light-source is switched off ($G = 0$). The carrier density $\Delta n(t)$ is schematically plotted in Fig. 1 together with the generation rate $G(t)$ for a square-wave modulated excitation.

Similar to photoconductance decay (PCD) measurements, τ_{eff} is obtained from the evaluation of the time-dependent behavior of Δn. Instead of monitoring the complete time-dependence of $\Delta n(t)$, one might investigate the ratio of two PL images. The first image is captured after switching on the light source and the second is captured under steady-state conditions. This simple ratio only depends on the camera integration time t_{int} and the effective carrier lifetime τ_{eff} for a linear relation between Δn and measured signal as shown in Ref. 8. Unfortunately, for the quadratic dependence of the PL signal on Δn the simple ratio of two PL images becomes a function of N_{dop} and G. However, the situation is different when applying an extended approach and

considering not only the increase of $\Delta n_{\text{rise}}(t)$, but also taking into account the decrease of $\Delta n_{\text{fall}}(t)$. According to the approach in Ref. 8, we introduce the parameter P:

$$P = \frac{\displaystyle\int_0^{t_{\text{int}}} \Delta n_{\text{rise}}(t)\,dt - \int_0^{t_{\text{int}}} \Delta n_{\text{fall}}(t)\,dt}{\displaystyle\int_{t_{\text{stst}}}^{t_{\text{stst}}+t_{\text{int}}} \Delta n_{\text{rise}}(t)\,dt} = \frac{\text{Im}_1 - \text{Im}_3}{\text{Im}_2 - \text{Im}_4}.$$

(3)

Im_1, Im_2, Im_3, and Im_4 label the four PL images, required for the experimental determination of P. The acquisition times for these four PL images are marked in Fig. 1. The increasing $\Delta n_{\text{rise}}(t)$ is recorded in the first image and the decreasing $\Delta n_{\text{fall}}(t)$ in the third image. For the numerator of P in Eq. (3) the difference between the first and third images is calculated. The denominator results from the difference between the steady-state signal of the second image, acquired at t_{stst}, and the constant background signal of the fourth image. For PL measurements, the quadratic dependence on Δn (Eq. (1)) has to be considered:

$$P = \frac{\displaystyle\int_0^{t_{\text{int}}}\left(\Delta n_{\text{rise}}^2 + N_{\text{dop}}\Delta n_{\text{rise}}\right)dt - \int_0^{t_{\text{int}}}\left(\Delta n_{\text{fall}}^2 + N_{\text{dop}}\Delta n_{\text{fall}}\right)dt}{\displaystyle\int_{t_{\text{stst}}}^{t_{\text{stst}}+t_{\text{int}}}\left(\Delta n_{\text{rise}}^2 + N_{\text{dop}}\Delta n_{\text{rise}}\right)dt} \dots$$

$$\dots = \frac{t_{\text{int}} + 2\tau_{\text{eff}}\exp\left(-\dfrac{t_{\text{int}}}{\tau_{\text{eff}}}\right) - 2\tau_{\text{eff}}}{t_{\text{int}}}.$$
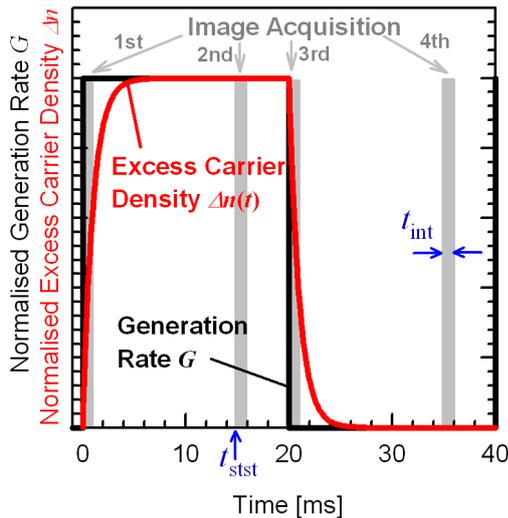
(4)

Figure 1: Time-dependent behavior of the excess carrier density Δn and the generation rate G for a square-wave modulated excitation. The grey bars mark the times of the image acquisition necessary for the dynamic lifetime evaluation.

Note that despite the quadratic dependence of the PL signal on Δn, P has the same τ_{eff}-dependence as obtained

for the linear relation between infrared emission and Δn in Ref. 8. The most important step in the calculation of Eq. (4) is the cancellation of N_{dop} and G. For that reason, the carrier lifetime can still be determined from the measurement of P for a known camera integration time but without the knowledge of any wafer parameters. The carrier lifetime is obtained locally, for each PL image pixel, by comparing the experimentally determined ratio P with the simulated ones. In Fig. 2, P is shown as a function of the carrier lifetime τ_{eff} for different camera integration times t_{int}.
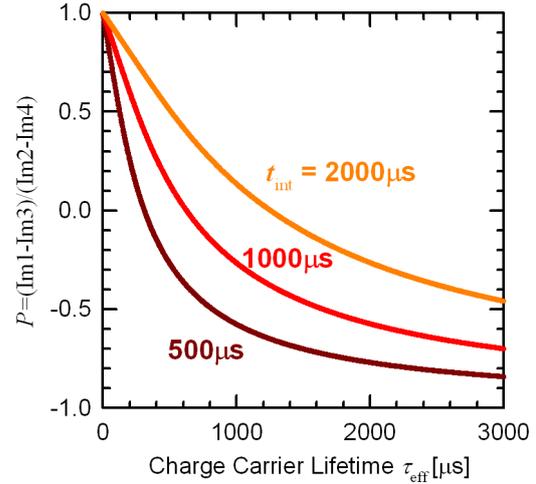

Figure 2: P from Eq. (4) in dependence on the carrier lifetime τ_{eff} for different camera integration times t_{int}.

Another interesting aspect arises from using P instead of the simple ratio of two PL images. One would expect a difference between the dynamically determined carrier lifetime and the steady-state lifetime for an injection-dependent lifetime. Interestingly, the impact of an injection-dependence of τ_{eff} on the dynamically determined lifetime cancels out almost completely as shown in Ref. 13 for a linear relation between measured signal and Δn. In this work, we give an experimentally verification by comparing steady-state and dynamic PL measurements in section 4 (Fig. (5)).

3 EXPERIMENTAL SETUP

A schematic of the experimental setup is shown in Fig. 3. We use an indium gallium arsenide (InGaAs) complementary metal-oxide semiconductor (CMOS) camera for the detection of the luminescence emission with a detection range from 900 nm to 1700 nm. The wafer under test is placed above a light emitting diode (LED, 850 nm) array for the excitation of electron-hole pairs. A spatially homogeneous excitation deviating by $\pm 10\%$ on an area of $18 \times 18 \text{ cm}^2$ is obtained by using a diffusion disc between LEDs and investigated sample. The time constants, describing the switching behavior of the LEDs, are below 10 μs and are considered in the analytical calculation of P. Although the InGaAs detector is not sensitive to the central wavelength of the excitation source, blocking of excitation photons is required. In our setup, the silicon wafer itself serves as a filter for the

photons of excitation. For further reduction of the flux of excitation photons and for the prevention of stray light in the setup, an optical long pass filter is mounted in front of the camera lenses. The switching behavior of the light source and the precisely timed image acquisition are controlled by synchronous TTL signals from a frequency synthesizer.
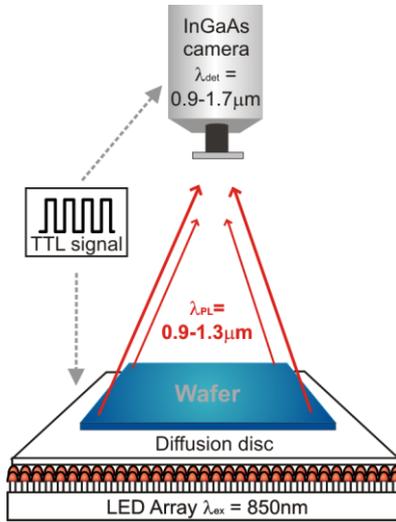

Figure 3: Schematic of the experimental setup for dynamic PL lifetime imaging.

4   MEASUREMENT RESULTS

In order to demonstrate the applicability of the dynamic PL imaging technique, we apply it to a 10×10 cm^2 SiN$_x$-passivated mc-Si wafer. Figure 4 (a) shows a dynamic PL image of the investigated wafer at an illumination intensity of 0.5 suns. The total measurement time is 32 s (8 s per image) for a modulation frequency of 25 Hz and 200 measurement periods for each image. The camera integration time for the single PL image is set at $t_{int} = 1$ ms. For comparison, we measure the carrier lifetime of the same wafer using the light-biased microwave-detected photoconductance-decay (MW-PCD) technique. The total acquisition time for the MW-PCD lifetime mapping is 90 min. The result of this measurement is shown in Fig. 4 (b).

Comparing both measurements by linescans we observe a good agreement in the regions of high lifetimes and deviations in regions of lower lifetimes The increased lifetimes determined in the low-lifetime regions of the dynamic PL measurement results from carrier diffusion and internal reflection of luminescence photons from regions of strong to regions of low PL emission, the so-called blurring effect [13]. This effect has a stronger impact on the dynamic evaluation than on the steady-state measurement. Therefore, Ramspeck et al. [13] suggested calibrating the steady-state image (2nd image in Fig. 1) using the dynamic lifetime image in a high-lifetime region of the wafer. In Fig. 4 (d), we show the result of this dynamically calibrated steady-state lifetime image. In Fig. 4 (c), we compare linescans of the three images and see a good quantitative agreement between the dynamically calibrated lifetime and the lifetime values from the MW-PCD lifetime mapping.
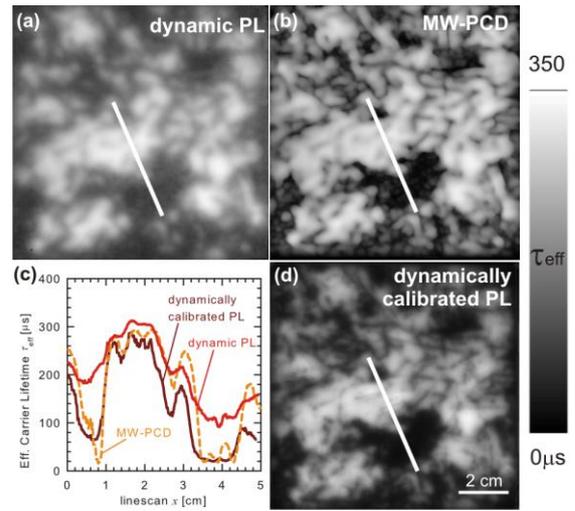

Figure 4: (a) Dynamic PL lifetime image of a 10 x 10cm^2 SiN$_x$-passivated mc Si wafer (measurement time: 32 s, spatial resolution ~210 μm). (b) MW-PCD lifetime mapping of the same wafer (measurement time: 90 min, step width: 250 μm). (c) Comparison of linescans of all three images, marked by the white lines, for quantitative comparison with the MW-PCD lifetime values. (d) A PL image in steady-state is calibrated using the dynamic PL image in the region of high lifetime.
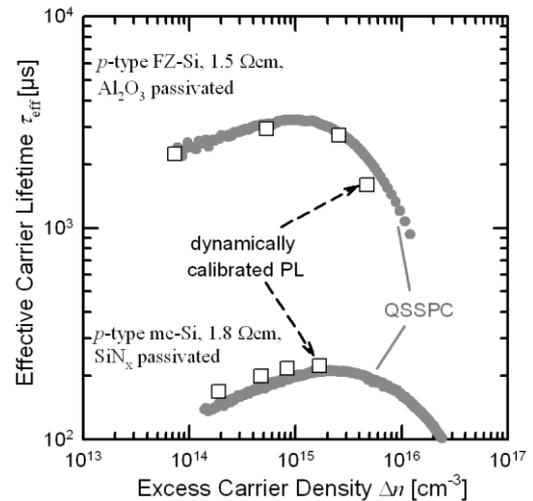

Figure 5: Injection-dependent effective lifetime τ_{eff} measured with dynamic PL lifetime imaging (open squares) and QSSPC (grey circles) for a *p*-type Al$_2$O$_3$-passivated FZ-Si wafer and a *p*-type SiN$_x$-passivated mc-Si wafer.

Additional comparative measurements were performed by using the quasi steady-state photoconductance decay technique (QSSPC) for injection-dependent carrier lifetime measurements. We investigated a 10×10 cm^2 Al$_2$O$_3$-passivated float-zone silicon (FZ-Si) wafer and the mc-Si wafer, shown in Fig. 4. The results from the QSSPC measurement are presented in Fig. 5 together with data points, extracted from dynamic PL lifetime images by averaging over the detection area (~18×18 mm^2) of the QSSPC setup in the center of the

wafer. To obtain the information of the excess carrier density $\Delta n = \tau_{eff} G$ from the dynamic PL lifetime image, we need indeed some wafer parameter to calculate the generation rate G. G is calculated from the excitation photon flux Φ according to $G = \Phi (1 - R) / W$ with W being the thickness and R the reflectivity of the wafer under test. Both lifetime techniques are in excellent agreement.

5 SENSITIVITY ANALYSIS

The parameter P from Eq. (4) only depends on the carrier lifetime τ_{eff} and the camera integration time t_{int}. Therefore, the integration time is an important parameter for the sensitivity of the dynamic PL lifetime technique. The impact of the noise behavior of the InGaAs detector on the determination of the lifetime with Eq. (4) is analyzed. The simulated relative uncertainty $\Delta\tau_{eff}/\tau_{eff}$ reflects the dependence of P on τ_{eff} and t_{int} and is shown in Fig. 6 as a function of t_{int}.

The expected PL signal for a fixed pair of τ_{eff} and t_{int} is simulated for all four images and inserted into Eq. (3). The relative uncertainty is calculated by determining the carrier lifetime from the PL signal plus/minus the statistical error due to the noise behavior of the used detector. The noise behavior of the InGaAs camera is analyzed and yields a $1/t_{int}$-dependence for the relative statistical uncertainty $\Delta I_{PL}/I_{PL}$ in the investigated range.

The uncertainty in τ_{eff} is calculated for carrier lifetimes of 30, 100 and 300 µs. The assumed number of averages M for each image is 200. The generation rate G is calculated for an illumination intensity of 0.5 suns, a wafer thickness of 200 µm and a wafer resistivity of 1.8 Ωcm and is the same for all three lifetimes.
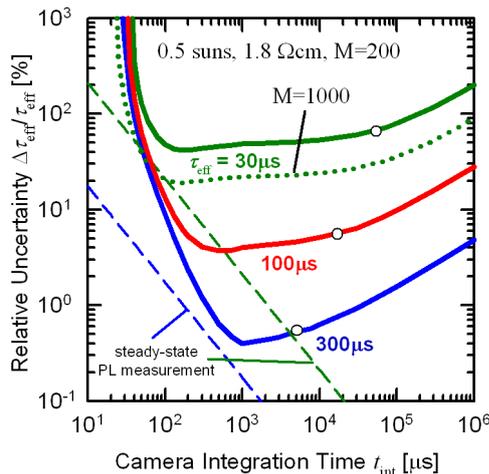

Figure 6: Relative uncertainty $\Delta\tau_{eff}/\tau_{eff}$ of the dynamic PL lifetime imaging technique for different carrier lifetimes τ_{eff} in dependence on the camera integration time t_{int}. The uncertainty is calculated for a constant generation rate and 200 averages per image. The dotted line shows $\Delta\tau_{eff}/\tau_{eff}$ for $\tau_{eff} = 30$ µs and 1000 averages per image. The open circles mark the integration time which leads to a saturated detector. The dashed lines show the uncertainty of the steady-state PL measurement.

We observe a minimum in the relative uncertainty for each carrier lifetime. For large $(t_{int} > \tau_{eff})$ and small $(t_{int} < \tau_{eff})$ camera integration times, the determined uncertainty increases due to the small difference between numerator and denominator in Eq. (3). For an mc-Si wafer with spatially distributed lifetime values, a compromise has to be accepted for the choice of the best suitable t_{int}. For the simulated scenario, lifetimes down to $\tau_{eff} = 30$ µs can be determined with an error < 20 % by increasing M to 1000 which corresponds to a total measurement time of 160 s (40 s per image).

For the presented measurement in Fig. 4, we minimize the uncertainty by dynamically calibrating the steady-state image. The uncertainty of the steady-state measurement is plotted in Fig. 6 (dashed line) and is determined only by the noise behavior of the InGaAs detector. Therefore, the uncertainty of the dynamically calibrated steady-state PL lifetime image in Fig. 4 (d) is well below 10 % for all lifetime regions.

6 CONCLUSION

We presented a calibration-free approach for measuring absolute carrier lifetimes within seconds based on photoluminescence imaging. No information about specific wafer parameters such as thickness, dopant density or reflectivity is needed. Our dynamic PL approach was applied to an mc-Si and a FZ-Si wafer. The results are in excellent agreement with an MW-PCD lifetime mapping and with injection-dependent QSSPC measurements. An analysis of the sensitivity of the dynamic PL approach was presented. It was demonstrated that for every carrier lifetime an optimal camera integration time exists for minimizing the uncertainty in τ_{eff}. From this analysis, we concluded that lifetimes can be reliably measured with a systematic error below 20 % down to 30 µs for a measurement time of 160 s and an illumination intensity of 0.5 suns. Note, that the total measurement time can be further reduced (quartered) by fully automatizing the experimental setup and acquiring all four images, needed for the dynamic evaluation, in one period of the modulated excitation.

REFERENCES

[1] T. Trupke, R. A. Bardos, M. C. Schubert, and W. Warta, Appl. Phys. Lett. **89**, 044107 (2006).
[2] M. The, M. C. Schubert, W. Warta, Proceedings of the 22nd European Conference on Photovoltaics Solar Energy Conversion, Milan, 2007, p. 354.
[3] S. Herlufsen, J. Schmidt, D. Hinken, K. Bothe, and R. Brendel, phys. stat. sol. (RRL) **2**, 245-247 (2008).
[4] T. Trupke, R.A. Bardos, and J. Nyhus, Proceedings 18th Workshop on Cryst. Silicon Solar Cells & Modules, Vail, USA, 2008, p. 88.
[5] J. A. Giesecke, M. Kasemann, and W. Warta, J. Appl. Phys. **106**, 014907 (2009).

[6] D. E. Kane and R. M. Swanson, Proceedings of the 18th IEEE Photovoltaic Specialists Conference, Las Vegas, USA, (IEEE, New York, 1985), p. 578.

[7] M. Kunst and G. Beck, J. Appl. Phys. 63, 1093 (1988).

[8] K. Ramspeck, S. Reissenweber, J. Schmidt, K. Bothe, and R. Brendel, Appl. Phys. Lett. **93**, 102104 (2008).

[9] D. Macdonald and A. Cuevas, Appl. Phys. Lett. **74**, 170 (1999)

[10] R. A. Bardos, T. Trupke, M. C. Schubert, and T. Roth, Appl. Phys. Lett. **88**, 053504 (2006).

[11] M. Bail, M. Schulz, and R. Brendel, Appl. Phys. Lett. **82**, 757 (2003).

[12] S. Herlufsen, J. Schmidt, D. Hinken, K. Bothe, R. Brendel, Proceedings of the 24th European Conference on Photovoltaics Solar Energy Conversion, Hamburg, Germany, 2009, p. 913.

[13] K. Ramspeck, K. Bothe, J. Schmidt, and R. Brendel, J. Appl. Phys. **106**, 114506 (2009).